

1 **Editor Comments to the Author:**

2

3 Dear Friedrich and coauthors,

4

5 Thanks for submitting the revised manuscript, which I will recommend for publication after
6 a very minor improvement: In the opening sentence of the introduction, you refer to
7 processes [not being preserved] in the rock record, an important theme. However, your
8 transition into garnet as a recorder of such processes is somewhat abrupt. Could you pick
9 this theme up just before the bullet list at the end of the introduction to introduce the list?

10

11 Further, lines 232-240 in the revised paper: Please shorten and restrict to what is directly
12 relevant to your research question.

13

14 Thanks a lot,

15 Florian

16

17 **Author response to Editor comments:**

18

19 Dear Florian,

20

21 Thank you for your recommendation of publication with very minor revisions and for your
22 suggestions with regard to those minor improvements. We agree that the transition in the
23 lines following line 82 were too abrupt and have expanded the section immediately before
24 the bullet points as follows:

25

26 Garnets can retain their microstructure and chemical composition during retrograde
27 deformation and metamorphism and can therefore preserve indicators for seismic events,
28 which are otherwise possibly erased from the rock record. Here we present a study of
29 garnet microstructures from lower crustal rocks of the Musgrave Block in Australia, which:
30 [...]

31

32 For the lines 232-240, we would argue that this description of the observed fracture sets is
33 already concise (indeed only 8 lines) and crucial to our later interpretation. It is necessary to
34 establish the existence of the late set II extensional fractures and the latter sentences are
35 simply a description of the fracture distribution and microstructure seen in Fig 5c.

36 This description is necessary in the text to highlight to the reader what we believe are the
37 most important features of the microstructure visible in 5c.

38

39 very best regards,

40 Friedrich and coauthors

41

42

43 We want to thank Matthias Konrad-Schmolke for his critical review and suggestions. Below is a list of
44 all comments from the reviewer (RC), answers from the authors (AC) and manuscript changes (MC).

45

46 **Reviewer 1, general comment**

47 **RC:** One crucial argument for crystal plasticity in garnet is the observation of dislocation walls that
48 mark the boundary of one subgrain in the garnet crystals. The authors state that these dislocation
49 walls are the result of dislocation climb in the crystal (lines 252-253) and therefore indicate the
50 activity of viscous deformation mechanisms in garnet. I am not entirely convinced that these
51 dislocation walls are only produced by the migration of dislocations through the crystal, although I
52 am not aware of studies that demonstrate neither pro nor contra arguments. The fact that the
53 authors do not cite any references is also not helpful with this regard. However, there is evidence
54 that such dislocation walls can be generated in undeformed rocks, e.g. during fluid infiltration, such
55 as demonstrated in Konrad-Schmolke et al., 2018. Of course, fluid infiltration does not play a role in
56 the rocks presented here, but other mechanisms for the formation of the dislocation walls must be
57 discussed in this manuscript, as these structures are a fundamental argument for crystal plasticity.
58 Furthermore, the interpretation of the presence of rotated subgrains in terms of subgrain rotation
59 recrystallization is, in my opinion, also questionable. Konrad-Schmolke et al., 2007 demonstrate the
60 presence of subgrains in garnets (and their slight misorientations) in undeformed rocks. In general, I
61 think that the manuscript would very much benefit from a more indepth discussion of these
62 features. The papers cited in this review should only serve as examples and I think that there are
63 many other contributions to the topic that I am not aware of at the moment. However, I think the
64 manuscript is very well suitable for publication after moderate revisions and a more thorough
65 discussion.

66 **AC:** As noted by the reviewer, fluid infiltration does not play a role in the rocks presented here, so
67 the mechanism proposed in Konrad-Schmolke et al., 2018 cannot be relevant in this case. The rocks
68 we are considering here are also clearly deformed, with stresses being high enough (at least
69 transiently) to cause fracturing of garnet. Progressive subgrain rotation by migration of dislocations
70 into walls bounding such subgrains is a mechanism that has been very widely proposed both in the
71 material and earth sciences. There is a large body of published work supporting and describing this
72 mechanism – indeed as noted by the reviewer “I think that there are many other contributions to
73 the topic”. It is not the aim of the current manuscript to provide an exhaustive review be we have
74 now added the following additional references as a representative selection:

75 Hobbs, B.E.: Recrystallisation of single crystals of quartz. *Tectonophysics*, 6, 353-401, 1968.

76 Passchier, C.W., Trouw, R.A.J.: *Microtectonics* (2nd Edition), Springer, Heidelberg, 366 pp., 2005.

77

78 **Reviewer 1, specific comments**

79 **RC:** Line 138: if the fractures a dilatant there must be some material in the cracks. Can that be
80 evaluated?

81 **AC:** No, these fractures remain empty, as implied by the word “unfilled” in the original text. These
82 fractures are Mode 1 extensional fractures, which we think open during propagation of the seismic
83 wave and immediately close, preventing any mineral filling.

84 **MC:** The word “dilatant” is perhaps better replaced with “extensional”, so the text now reads “*An*
85 *apparent late generation of unfilled extensional fractures [...]*”. All other similar references to
86 “dilatant fractures” have also now been changed to “extensional fractures”.

87

88 **RC:** What about the other, fast diffusing elements, such as Mn and Mg? Differences in diffusion
89 lengths would indicate different diffusion velocities and thus support the idea of a diffusional
90 modification.

91 **AC:** In Figure 4 d) we present the profiles for Fe, Mg, Mn. Fe and Mg show the same diffusion length
92 as Ca. Mn does not show any measurable modification throughout the crystal.

93 **MC:** This observation was missing in the text, therefore we added the following sentence for
94 clarification: *“The length-scale for variation in Fe (X_{Alm}) and Mg (X_{Pyd}) is identical to that for Ca (X_{Grs}),*
95 *whereas the Mn content (X_{SpS}) does not show any variation (Fig 4d).”*

96

97 **RC:** Lines 196-197: This diffusional modification is likely due to subgrain boundaries that might or
98 might not be associated with subgrain rotations. This has been demonstrated in Konrad-Schmolke et
99 al., 2007 (EJM). This should be discussed or at least mentioned.

100 **AC:** Since a subgrain is defined by a relative crystallographic rotation (commonly taken arbitrarily as
101 between ca. 4° and 15°, when it is considered to be a “high-angle boundary” to a “new grain”, e.g.
102 Urai et al., 1986), the generally accepted argument is that subgrain boundaries are always associated
103 with subgrain rotations, as new dislocations are continuously added to the subgrain boundaries (e.g.
104 Passchier and Trouw, 2005, p.43). We have added the reference to Konrad-Schmolke et al. (2007), as
105 well as recent publications of Petley-Ragan et al. (2019), Jamtveit et al. (2018a,b, in press), Engi et al.
106 (2018), Giuntoli et al. (2018) and Angiboust et al. (2017) when comparing and contrasting our “dry”
107 results to fracture and diffusion in garnets in deep-seated rocks where fluid infiltration plays an
108 important role.

109

110 We want to thank the anonymous reviewer for his critical review and suggestions. Below is a list of
111 all comments from the reviewer (RC), answers from the authors (AC) and manuscript changes (MC).

112

113 **Reviewer 2, general comment**

114

115 **RC:** The main message of this manuscript is the occurrence of crystal plasticity in garnet at
116 temperatures well below the laboratory derived data for the onset of crystal plastic deformation in
117 garnet. The authors, therefore, state that laboratory data fail to explain the natural observations. Of
118 course laboratory experiments are most often very simplified rendering extrapolation to natural
119 systems rather challenging. Though, I miss a bit the explanation why the laboratory data does not
120 match natural observations. Is it because the samples in the laboratory were even drier than the
121 natural rock delaying the onset of crystal plastic deformation in the laboratory? Obviously there
122 were some fluids present due to the occurrence of biotite. Though in some parts of the manuscript,
123 the authors state that a Ca-rich garnet forms instead of epidote, because of the low water activity
124 (line 290). Perhaps there was enough water around to facilitate crystal plastic deformation but not
125 enough to stabilize epidote? I think it would improve the manuscript to discuss the role of fluids on
126 crystal plastic deformation in more detail. This might also explain the discrepancy between
127 laboratory data and the natural observations.

128 **AC:** We have added text in several places to expand the discussion of the apparent discrepancy with
129 laboratory data, in particular considering the potential effects of strain rate and role of fluids. We
130 agree that this should have been treated in more detail, which is why we now have a rather more
131 nuanced approach, considering factors that may have an influence rather than just stating that there
132 is a difference.

133

134 **RC:** Line 71: In this context I think crystal plastic deformation instead of ductile deformation is more
135 appropriate.

136 **AC:** agree

137 **MC:** changed sentence: *"between brittle and crystal plastic deformation of garnet"*

138

139 **RC:** Lines 276-278: Did you investigate/find garnet crystals that were cut by a pseudotachylyte? Both
140 studies that you cite, Austrheim et al. (2017) and Papa et al. (2018), demonstrate garnet crystals that
141 are situated right next to a pseudotachylyte-bearing fault. I mention this, because as strain rate and
142 stresses decrease very rapidly with increasing distance, the required stresses and/or strain rates at a
143 few mm to the fault might not be sufficient anymore to extensively fragment garnet.

144 **AC:** In the text, we clearly state that *"Granulite facies garnet porphyroclasts in Musgravian*
145 *peraluminous gneisses mylonitized during the Petermann Orogeny are almost invariably fractured,*
146 *irrespective of their proximity to pseudotachylyte (Fig. 3)."* This is different than what was observed
147 in the examples of Austrheim et al. (2017) and Papa et al. (2018) mentioned above, which is why we
148 made such a clear statement originally. On the basis of this observation, we argue in the text that
149 the whole rock was affected by high stresses during transient seismic events and that garnet
150 fracturing is not restricted to the localized damage zone of a propagating fracture (Petley-Ragan et
151 al., 2019; Austrheim et al., 2017) or thermal shock immediately adjacent to the high temperature
152 pseudotachylyte (Papa et al., 2018).

153

154 **RC:** Line 286: Delete 'of some'.

155 **AC:** agree

156 **MC:** Typing error corrected.

157

158 **RC:** Lines 291-292: So everything is dry, but suddenly there is biotite? You should discuss the
159 presence/absence of hydrous minerals a bit more.

160 **AC:** Biotite is a typical mineral of granulite facies assemblages up to the point of melting (with biotite
161 then providing the water for "anhydrous" melting) and even then biotite is a common mineral in the
162 restite assemblage. "Kinzigite", which is a typical "dry" lower-crustal granulite facies rock, is actually
163 defined as having garnet + biotite. As noted by Pennacchioni and Cesare (1997), under upper
164 amphibolite facies conditions, newly grown biotite can actually act as a sink for any free water
165 available and the same will be true for the "dry" high pressure upper amphibolite ("sub-eclogitic")
166 facies conditions relevant to the current study.

167 Pennacchioni, G. & Cesare, B., 1997. Ductile-brittle transition in pre-Alpine amphibolite facies
168 mylonites during evolution from water-present to water-deficient conditions (Mont Mary nappe,
169 Italian Western Alps). Jour. Metm. Geol. 15, 777-791.

170

171 **RC:** Lines 304-305: Shimada et al. (1983) experimentally investigated that the angle changes from
172 around 30 to approx. 45° with increasing pressure.

173 **MC:** The reference was added to the text: *“This plot is only qualitative, since the angle of internal*
174 *friction could decrease towards higher pressure (Shimada et al., 1983).”*

175

176 **RC:** Lines 311-313: See comment above. As water seems important you should perhaps quantify the
177 amount of water? There is some water present in the other field studies mentioned, but not very
178 much. How should the presence of a fluid help to fragment the rock?

179 **AC:** As noted already in Wex et al. (2018), for the relevant pressure and temperature conditions, the
180 presence of kyanite as the result of plagioclase breakdown, to the exclusion of clinozoisite / epidote,
181 implies a water activity of less than ca. 0.004, according to Wayte et al. (1989) (as is also noted again
182 in the current manuscript). The examples from Holsnoy all have extensive development of
183 clinozoisite during eclogite formation.

184

185 **RC:** Figure 5: The difference between fracture types I and II is not very clear to me. The magnification
186 at which the image was taken is quite low and therefore it is difficult to see subgrains.

187 **AC:** The step-size for this map was 2 micrometres, which is obviously a compromise due to the large
188 area of the garnet, and individual points are still visible in the figure. Unfortunately, we do not have
189 a higher resolution scan for the specific area. We hope that the subgrains are still visible as slight
190 changes in colour and grey-values, as seen and highlighted in the red area. We admit that there is no
191 genetic difference between the proposed fracture sets I and II and have therefore dropped any
192 differentiation between the two.

193 **MC:** Figure 5 was changed in regard to the labelling of the fractures and the text was changed
194 accordingly.

195

196

197

198 **MANUSCRIPT INCLUDING CHANGES**

199 **Fracturing and crystal plastic behaviour of garnet under seismic stress in the**
200 **dry lower continental crust (Musgrave Ranges, Central Australia)**

201

202

203 Friedrich Hawemann^{1*}, Neil Mancktelow¹, Sebastian Wex¹, Giorgio Pennacchioni², Alfredo
204 Camacho³

205 1) Department of Earth Sciences, ETH Zurich, CH8092 Zurich, Switzerland

206 2) Department of Geosciences, University of Padova, Padova, Italy

207 3) Department of Geological Sciences, University of Manitoba, Winnipeg, Manitoba, R3T
208 2N2, Canada

209 * corresponding author friedrich.hawemann@erdw.ethz.ch

210

211 **Highlights**

- 212 • garnet deformed by fracturing and crystal-plasticity under dry lower crustal conditions
- 213 • Ca-diffusion profiles indicate multiple generations of fracturing
- 214 • diffusion is promoted along zones of higher dislocation density
- 215 • fracturing indicates transient high-stress (seismic) events in the lower continental
216 crust

217 **Abstract**

218 Garnet is a high strength mineral compared to other common minerals such as quartz and
219 feldspar in the felsic crust. In felsic mylonites, garnet typically occurs as porphyroclasts that
220 mostly evade ~~intracrystalline~~crystal-plastic deformation, except under relatively high
221 temperature conditions. The microstructure of granulite facies garnet in felsic lower-crustal
222 rocks of the Musgrave Ranges (Central Australia) records both fracturing and crystal-plastic
223 deformation. Granulite facies metamorphism at ~ 1200 Ma generally dehydrated the rocks
224 and produced mm-sized garnets in peraluminous gneisses. A later ~ 550 Ma overprint under
225 sub-eclogitic conditions (600-700 °C, 1.1-1.3 GPa) developed mylonitic shear zones and ~~with~~
226 abundant pseudotachylyte, coeval with the neocrystallization of fine-grained, high-calcium
227 garnet. ~~In the mylonites, The granulite-facies~~ fractured garnet porphyroclasts ~~in mylonites~~
228 ~~show have high~~are enriched in calcium ~~content~~ along rims and fractures. However, ~~in certain~~
229 ~~cases,~~ these rims are locally narrower than ~~equivalent otherwise comparable~~ rims along
230 original grain boundaries, indicating contemporaneous diffusion and fracturing of garnet. The
231 fractured garnets exhibit internal crystal-plastic deformation, ~~that which~~ coincides with areas
232 of enhanced diffusion, usually along zones of crystal lattice distortions and dislocation walls
233 ~~and by~~associated with subgrain rotation recrystallization. Fracturing of garnet under dry
234 lower crustal conditions, in an otherwise viscously flowing matrix, requires transient high
235 differential stress, most likely related to seismic rupture, consistent with the coeval
236 development of abundant pseudotachylyte.

237

238 **Keywords**

239 Garnet, Fracture, Crystal-Plasticity, Dry Lower Continental Crust, Pseudotachylyte, Seismicity

240 **1 Introduction**

241 A fundamental problem in geology is the limited preservation of processes in the rock record.
242 This is especially the case for transient events, like earthquakes, traces of which are hardly
243 preserved due to later reworking. The best indicators for seismicity in the rock record are
244 pseudotachylytes (Sibson, 1975; Toy et al., 2011), although not every seismic event produces
245 frictional melts and, once formed, ductile creep or later brittle fracturing may erase most
246 traces (Sibson and Toy, 2006; Kirkpatrick and Rowe, 2013).

247 Garnet is stable in many metamorphic rocks over a large part of the pressure-temperature
248 space, is commonly preserved, and is suitable for a range of geothermobarometers and
249 geochronometers and their combination for geospeedometry (Lasaga, 1983; Caddick et al.,
250 2010; Baxter and Scherer, 2013). Being a high strength mineral (Karato et al., 1995; Wang and
251 Ji, 1999), both brittle and crystal plastic deformation are rarely observed in garnet when
252 compared to the common matrix minerals of the crust, such as quartz and feldspar. However,
253 Dalziel and Bailey (1968) already interpreted elongate garnets in a-high grade mylonites as to
254 be the result of crystal plastic ~~behavior~~behaviour. ~~and Advancements~~advancements since
255 then in electron microscopy, and especially EBSD (electron backscatter diffraction), have
256 allowed detailed investigation of garnet textures (Kunze et al., 1993; Prior et al., 2000, 2002).

257 Experimental deformation of garnet indicates that differential stresses on the order of a few
258 GPa are required to produce shear fractures (~~Wang and Ji, 1999~~), and that the onset of ductile
259 crystal plastic ~~behavior~~behaviour for strain rates typical of actively deforming regions (10^{-12} –
260 10^{-15} s⁻¹; e.g. Behr and Platt, 2011) should only occurs at corresponding temperatures above
261 ca. 750-640 850 °C (Karato et al., 1995; Wang and Ji, 1999). The observation of fractured
262 garnets in natural samples may therefore be linked to seismic stresses, as suggested by

263 Austrheim et al. (1996), who described fracturing of garnets during pseudotachylyte
264 formation and fluid-assisted eclogitization of granulites. Trepmann and Stöckhert (2002) also
265 interpreted the microstructure of fractured and offset garnets as evidence for syn-seismic
266 loading and post-seismic creep. ~~In addition, and, m. More recently, Austrheim et al. (2017)~~
267 ~~again also associated both~~ brittle (Austrheim et al., 2017; Engi et al., 2017; Angiboust et al.,
268 2017; Giuntoli et al., 2018; Hawemann et al., 2018; Petley-Ragan et al., 2019) and associated
269 crystal-plastic ~~behavior~~ behaviour (Austrheim et al., 2017; Petley-Ragan et al., 2019) of garnets
270 ~~has been related to~~ with lower crustal seismic events in lower continental crust or deeply
271 ~~subducted continental fragments~~. Papa et al. (2018) interpreted similar deep-seated dilatant
272 fracturing of garnet immediately adjacent to pseudotachylyte to be related to thermal shock
273 due to frictional heating rather than to damage associated with propagation of the seismic
274 rupture. ~~Konrad-Schmolke et al. (2007) described enhanced diffusion of Mg along subgrain~~
275 ~~boundaries in garnet (but not of slow diffusing elements, such as Ca, Ti and Y) from meta-~~
276 ~~granitoid high pressure meta-granitoid rocks of the deeply subducted Sesia Zone (Western~~
277 ~~Alps).- However, in contrast to more recent studies in the Sesia Zone, which propose that~~
278 ~~precursor fracturing was crucial for dissolution-precipitation and diffusion processes in~~
279 ~~garnet (Engi et al., 2018; Giuntoli et al., 2018), they considered that there were no signs of~~
280 ~~crystal-plastic deformation in their garnet samples and concluded that a diffusion-induced~~
281 ~~dislocation migration and/or diffusion-induced recrystallisation process was responsible for~~
282 ~~development of the observed subgrain texture.~~
283 Garnets can retain their microstructure and chemical composition during retrograde
284 deformation and metamorphism and can therefore preserve indicators for seismic events,
285 which are otherwise possibly erased from the rock record. Here we present a study of garnet
286 microstructures from lower crustal rocks of the Musgrave Block in Australia, which:

- 287 (1) illustrates the close association between brittle and [ductile—crystal—plastic](#)
288 deformation of garnet under well-established pressure-temperature conditions;
289 (2) infers deformation mechanisms from the observed microstructure;
290 (3) explores the close link between deformation and diffusion in garnet;
291 (4) complements other independent observations indicating transient high stresses in the
292 lower crust.

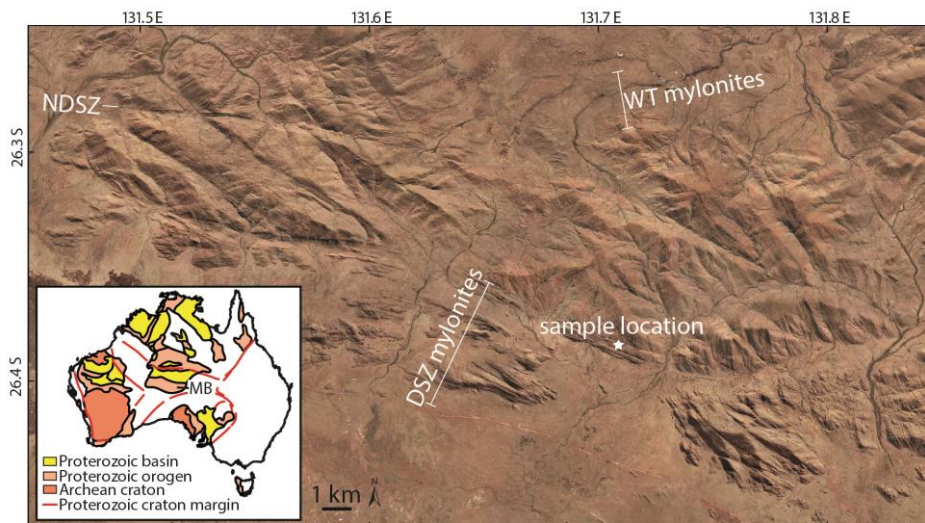
294 **2 Geological setting**

295 2.1 Regional geology

296 The Musgrave Block is located in an intraplate position close to the [centercentre](#) of the
297 Australian continent (inset Fig. 1). Amalgamation of the different cratonic blocks took place
298 during the Musgravian Orogeny (1120-1200 Ma), which pervasively overprinted ca. 1550 Ma
299 gneisses (Gray, 1978; Camacho and Fanning, 1995). The Petermann Orogeny (~550 Ma)
300 produced a series of crustal-scale fault zones, most prominently the Woodroffe Thrust and
301 the Mann Fault (Collerson et al., 1972; Major, 1973; Bell, 1978; Camacho and Fanning, 1995;
302 Raimondo et al., 2010; [Hawemann et al., 2018, 2019](#); Wex et al., 2017, 2018, 2019). The south-
303 dipping Woodroffe Thrust has a top-to-the-north sense of shear, and juxtaposes the Fregon
304 Subdomain in the south (hanging wall) against the Mulga Park Subdomain in the north
305 (footwall). During the Musgravian Orogeny, the Mulga Park Subdomain attained amphibolite
306 facies conditions while the Fregon Subdomain reached granulite facies (Camacho and
307 Fanning, 1995; Scrimgeour et al., 1999; Scrimgeour and Close, 1999), and depleted the rocks
308 of OH-bearing minerals (Wex et al., 2018; Hawemann et al., 2018).

309 The Woodroffe Thrust hosts one of the largest occurrences of pseudotachylyte worldwide
310 (Camacho et al., 1995), but all larger scale shear zones in the hanging wall also show abundant
311 pseudotachylyte that developed under lower crustal conditions (Camacho, 1997; Hawemann
312 et al., 2018). Deformation in the Fregon Subdomain associated with the Petermann Orogeny
313 is concentrated along the sub-eclogitic (~650 °C, 1.2 GPa) Davenport Shear Zone and the
314 North Davenport Shear Zone (Fig. 1), with little discernible overprint of the earlier granulites
315 in between (Camacho et al., 1997). The Davenport Shear Zone is a WNW-ESE-striking, strike-
316 slip zone, with a near horizontal stretching lineation. Deformation inside the Davenport Shear
317 Zone itself is heterogeneous and strongly localized (Hawemann et al., 2019).

318



319

Figure 1: Airborne imagery of the study area with sample location (26.3849 S, 131.7067 E) in the Davenport Shear Zone (DSZ). NDSZ = North Davenport Shear Zone, WT = Woodroffe Thrust. Image from the Department of Primary Industries and Regions, South Australia (PIRSA), 2012. Inset: Location of the Musgrave Block (MB) in between the amalgamated Australian Cratons. Modified after Evins et al. (2010)

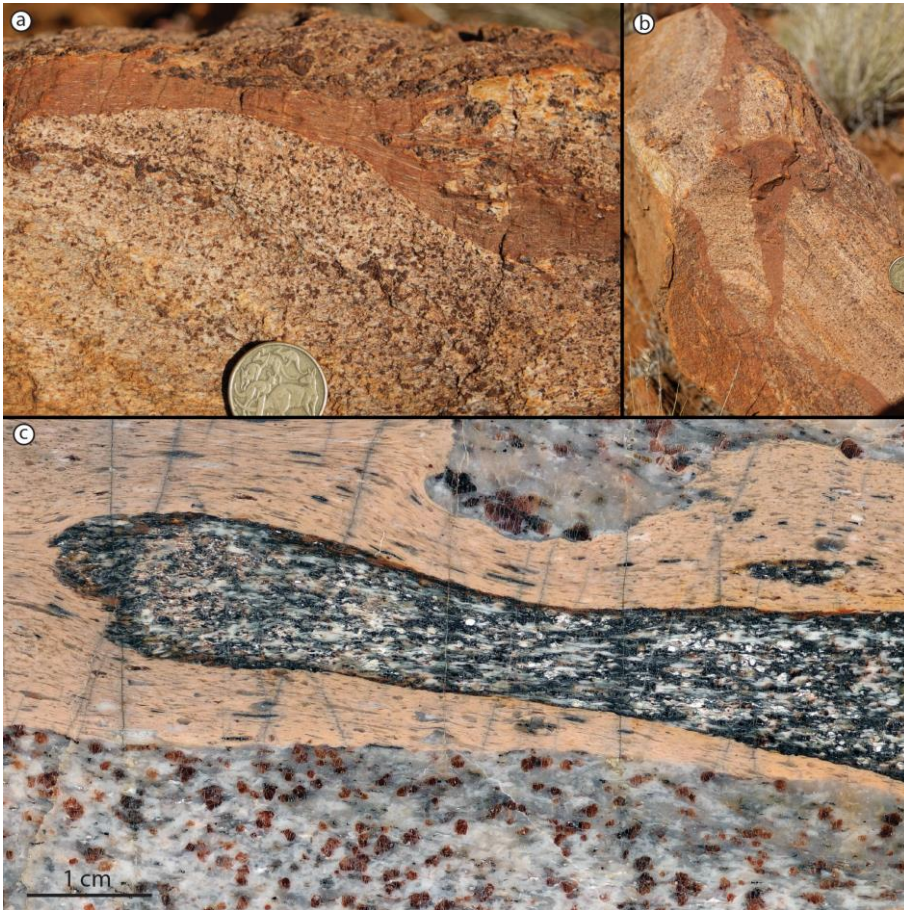
320

321 2.2 Sample description

322 Fractured garnet is ubiquitous in the Fregon Subdomain and is not exclusively found in
323 association with pseudotachylyte veins. However, this study focuses on a representative
324 outcrop for which field relationships, metamorphic, and deformation conditions have been
325 well established (F68, Hawemann et al., 2018; 26.3849 S, 131.7067 E). This outcrop consists
326 of a quartzo-feldspathic mylonite, with ~~millimeter~~millimetre-sized, granulite facies garnets,
327 ~~that and~~ includes multiple pseudotachylyte veins and breccias. Pseudotachylytes in the
328 studied outcrop are sheared, as indicated by elongated clasts (Fig. 2a, c), and show the same
329 stretching lineation as the host mylonite. The original discordant relationship to the host
330 foliation is still preserved, with the crosscutting relationship most obvious in sections and cuts
331 perpendicular to the stretching lineation (Fig. 2b).

332 The syn-mylonitic assemblage associated ~~to with~~ the Petermann overprint of the felsic
333 granulites is Qz+Kfs+Pl+Gt+Bt+Ky+Ilm+Rt (mineral abbreviations following Whitney and
334 Evans, 2010), and is similar to that of the associated sheared pseudotachylyte
335 (Qz+Kfs+Pl+Gt+Bt+Ky+Rt) (Hawemann et al., 2018). The fine-grained garnet growing within
336 the pseudotachylyte gives the rock its macroscopic ~~color~~colour ~~in macroscopic~~
337 ~~images~~—(Fig. 2). Fractured—Larger fractured garnets within the granulites are clearly
338 recognizable in polished hand specimens (Fig. 2c) and are very apparent in thin section (Fig.
339 3). The metamorphic conditions during shearing of this pseudotachylyte are estimated at ~600
340 °C and ~1.1 GPa (Fig. 7 of Hawemann et al., 2018).

341



342

Figure 2: Sheared pseudotachylyte in a view orthogonal to the foliation of host felsic mylonite, and looking perpendicular (a) and parallel (b) to the stretching lineation. c) Polished hand specimen of a sheared pseudotachylyte breccia with the caramel-coloured foliated pseudotachylyte matrix including elongated clasts and an elongate fragment of mafic granulite. The host rock shows millimetermillimetre-sized garnets with fractures. Plane of the polished surface is perpendicular to the foliation and parallel to the stretching lineation.

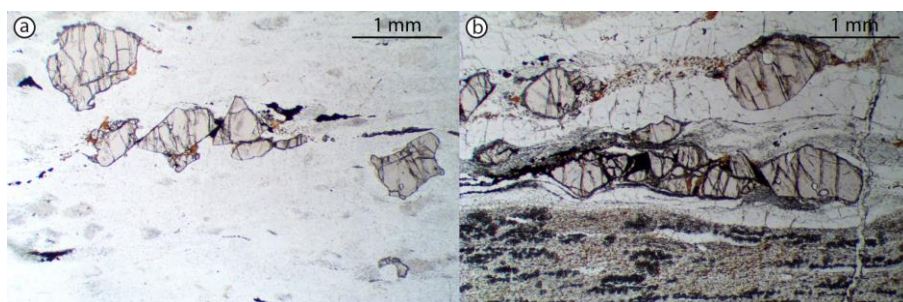
343

344 **3 Garnet microstructure and compositional variation**

345 3.1 Optical microstructure

346 Granulite facies garnet porphyroclasts in Musgravian peraluminous gneisses mylonitized
347 during the Petermann Orogeny are almost invariably fractured, irrespective of their proximity
348 to pseudotachylyte (Fig. 3). Large garnet porphyroclasts (>1 mm) are typically slightly
349 elongated with their long axis parallel to the foliation, which is attributed at least partially to
350 resorption. Fractures in garnets often show offsets ~~in~~on the order of a few 100 μm . It is not
351 possible to determine whether these offsets are primarily due to the initial shear fracture or
352 result from subsequent sliding during ongoing ductile shear. Moreover, no consistent sense
353 of shear can be derived from the offsets (Fig. 3a, b). These discrete fractures are sub-planar,
354 commonly have a consistent orientation at a moderate angle to the foliation, and locally occur
355 in conjugate sets (Fig. 3b). Wide fractures are filled with biotite, kyanite and quartz (Fig. 4b).
356 An ~~apparent~~ later generation of unfilled ~~dilatant~~ fractures, without any discernible offset, is
357 oriented perpendicular to both the foliation and stretching lineation (Fig. 3b). Garnet
358 porphyroclasts commonly contain rutile exsolution lamellae and inclusions of monazite and
359 kyanite (Fig. A1). The latter are present as aggregates with an overall prismatic shape, possibly
360 representing pseudomorphs after sillimanite (Camacho and Fitzgerald, 2010).

361



362

Figure 3: Thin section photomicrographs in plane polarized light of fractured garnets away from pseudotachylyte (a), and close to sheared and recrystallized pseudotachylyte in the lower part of the figure (b). The dark trails of grains elongated in the foliation of the sheared pseudotachylyte are small new garnets. Section is perpendicular to the foliation and parallel to the stretching lineation.

363

364

365

366 3.2 Analytical techniques

367 Quantitative mineral compositions were measured with a JEOL JXA-8200 electron probe
368 micro-analyzer (EPMA), equipped with a tungsten filament, at the Institute of Geochemistry
369 and Petrology at ETH Zurich (Switzerland). Natural standards were used for quantification,
370 and, when available, natural garnet standards were preferred. To reach a spatial resolution
371 of about 1 μm , an acceleration voltage of 10 kV was set (Fig. 8 in Hofer and Brey, 2007).

372 Elemental maps were acquired using energy wavelength-dispersive spectrometers in parallel
373 for calcium, to increase the signal-to-noise ratio. Backscatter electron images (BSE), energy-
374 dispersive spectrometry (EDS) and electron backscatter diffraction (EBSD) mapping was
375 carried out on a Quanta 200F field emission gun (FEG) scanning electron microscope at the
376 ScopeM (Scientific Center for Optical and Electron Microscopy, ETH Zurich). EBSD maps were
377 collected with an acceleration voltage of 20 kV, a sample tilt of 70° and a working distance of
378 15 mm. Data were post-processed using chemical indexing with the software OIM 7 by EDAX.

379 When necessary, three different clean-up techniques were used: ~~neighbor~~neighbour
380 confidence index correlation, ~~neighbor~~neighbour orientation correlation and grain dilation.

381 Point and map analyses, as well as BSE images, were combined for correlation with optical
382 microscope images in a QGIS-project (Open Source Geospatial foundation). Two lamellae
383 were cut with a focused ion beam (FIB) for transmission electron microscopy (TEM). The

384 microscope used for TEM is a Tecnai F30 with a FEG source operated at 300 kV and equipped
385 with a Gatan 794 MultiScan CCD (ScopeM, ETH Zurich).

386 3.3 ~~Compositional~~Compositional gradients

387 Granulite facies garnet has a homogeneous composition of X_{Alm} 0.54, X_{Pyp} 0.40, X_{Grs} 0.03, X_{Sps}
388 0.03, whereas garnet neocrystallized during the Petermann Orogeny is more Ca-rich (X_{Alm}
389 0.48, X_{Pyp} 0.28, X_{Grs} 0.22, X_{Sps} 0.02). Grain boundaries of granulite facies garnet and fractures
390 are decorated with a Ca-enriched rim, 20 to 40 μ m wide (Fig. 4c). ~~The enrichment is mostly
391 concentric, also affects resorbed areas of the garnet and is therefore most likely the result of
392 diffusion (Camacho et al., 2009). The length-scale for variation in Fe (X_{Alm}) and Mg (X_{Pyp}) is
393 identical to that for Ca (X_{Grs}), whereas the Mn content (X_{Sps}) does not show any variation (Fig
394 4d). The diffusion length for iron and magnesium is identical to Ca, while the manganese
395 content does not show any variations (Fig 4c).~~ Neocrystallized garnet is present where the
396 grain boundary is in contact with, or close to, plagioclase. The outermost rim of remnant
397 garnet has the same composition as the neocrystallized garnet (Fig. 4d, profile 1). The
398 ~~granulitic-granulite-facies~~ plagioclase is partially transformed to a more Na-rich plagioclase
399 with needle shaped inclusions of kyanite (bottom of Fig. 4e). This reaction provides Ca for the
400 observed diffusion into garnet (Camacho et al., 2009).

401 Along fractures across the porphyroclasts, the Ca enrichment is narrower than along the grain
402 boundaries and the grossular component only reaches up to about X_{Grs} 0.1 (Fig. 4d, profile 2).
403 Compositional gradients are also present around inclusions in garnet connected to the outer
404 garnet boundary, providing evidence of Ca diffusion along grain boundaries (right part of Fig.
405 4c, profile 3 in Fig 4d). Profile 4 (Fig. 4d) was measured next to a kyanite inclusion: the
406 diffusion length is still comparable to those of profiles 1-3, but Ca concentrations are much

Commented [n1]: This text is eliminated here because it is interpretation and best considered the discussion section below.

407 lower. Ca probably diffused along fractures (invisible in the plane of the thin section) towards
408 the inclusion. In summary, the diffusion length at the original grain boundaries is maximized
409 where in contact with plagioclase, and otherwise constant at about 20 μm width. However,
410 variations in diffusion lengths do occur around garnet fragments, without any correlation with
411 the proximity to plagioclase, although the exact relationship in the third dimension is
412 unknown. Surfaces with limited diffusion can often be identified as fracture surfaces, which
413 were exposed to diffusion for a shorter time than original grain boundaries (Fig. 4e). Fractures
414 oriented perpendicular to the foliation and stretching lineation lack any signs of diffusion and
415 are therefore interpreted as later stage ~~dilatant~~ extensional fractures.

416 Some garnets display more complicated compositional patterns, with zones $>100 \mu\text{m}$ of Ca
417 enrichment extending into the porphyroclast's interior, which are not associated with
418 fractures (e.g. the garnet fragment on the far right in Figure 4e). EBSD-analysis highlights that
419 the three fragments in the right part of Figure 4e most likely originated from the same grain,
420 as they share a common rotation axis (Fig. 4f). The ~~colors~~ colours in the inverse pole figure
421 map are not solid, reflecting slight variations of orientation within the crystal. Furthermore,
422 the image quality map shows areas of suppressed Kikuchi patterns (grey value) suggestive of
423 higher dislocation density and therefore possible subgrain boundaries (Fig. 4f). The
424 misorientation angle map (Fig. 4g) reveals a complex pattern of varying crystal orientation (all
425 within the order of 5°) in the fragments, with very distributed zones connected to the edges
426 of the crystal, triangular-shaped zones of misorientation (upper left of Fig. 4g), and discrete
427 zones (lower right of Fig. 4g). The discrete zones of misorientation, about $5 \mu\text{m}$ wide, correlate
428 well with the Ca-enriched zones (compare Fig. 4e, f, garnet fragment on the right).

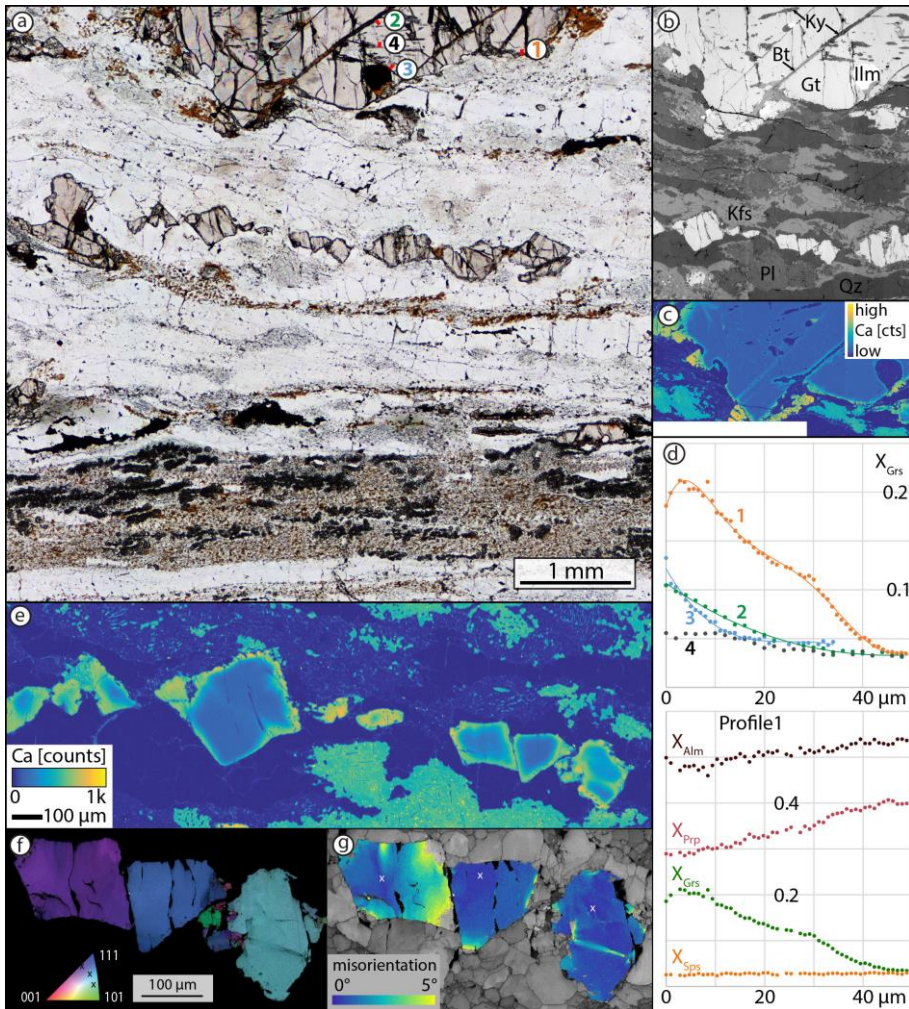


Figure 4: a) Plane polarized light image of thin section with fractured garnets and a pseudotachylyte vein in the lower part of the image. b) BSE image of the upper area of (a), with same scale as (a). c) EPMA X-ray map for Ca reveals an enrichment the-in thin diffusion gradational rims along grain boundaries, and fractures, and within neocrystallized garnet (euhedral, orange). d) Grossular component profiles indicated on (a) (Profile-profile lines are not to scale for the sake of visibility); and compositional profiles for four garnet end-members in profile 1. e) EPMA X-ray map for Ca for the garnet fragments in the center of (a). Note the uneven colours in the plagioclase and the blue kyanite needles. f) Inverse pole figure map with superimposed image quality map for garnet fragments shows a common rotation pole. g) Misorientation map relative to reference point for each fragment reveals internal lattice distortions.

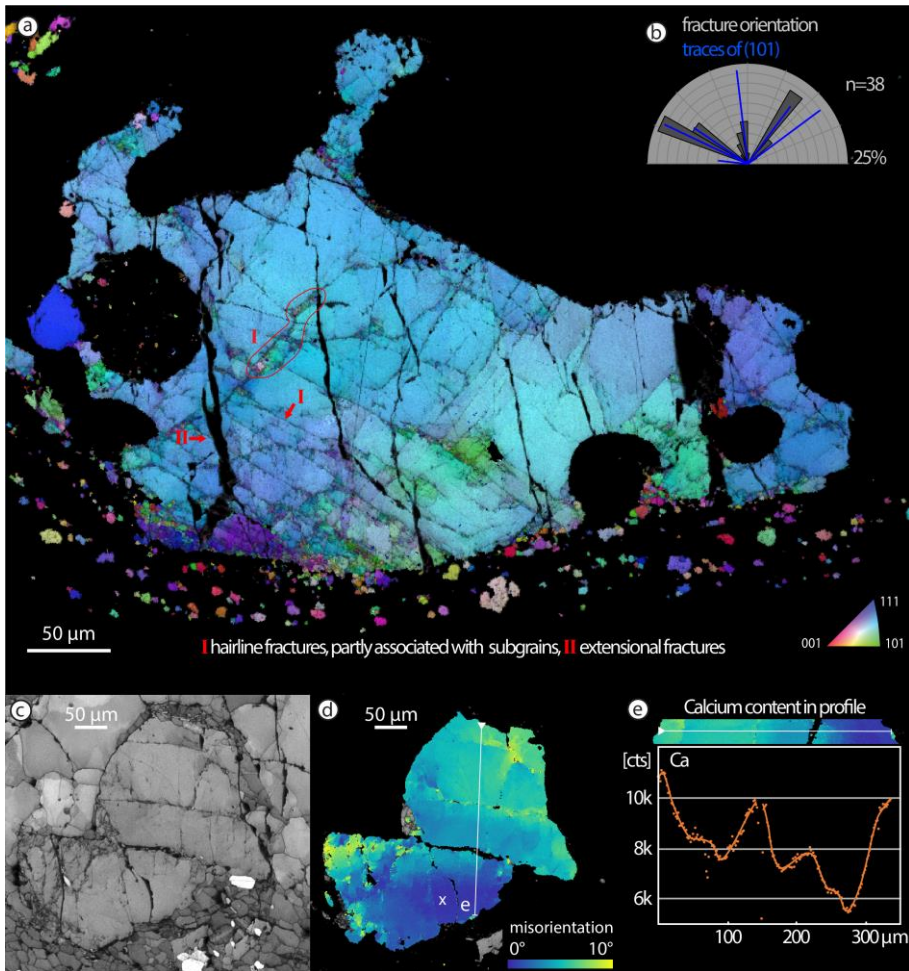
429

430

431 3.4 Texture of deformed garnets

432 Two to three orientations of fractures are generally present in a single garnet crystal and
433 coincide with the trace of the (101)-plane derived from EBSD data (Fig. 5a, b). Fracture set (I)
434 in the example of Figure 5a is often associated with a relative rotation of both sides, as visible
435 from the difference in ~~color~~colour. In the lower part of the grain, where the fracture density
436 is very high, more subgrains are present. The subgrain spatial density increases towards the
437 original grain boundary and some subgrains are “eroded” by ductile shearing and strung out
438 along the foliation. This demonstrates that ductile shearing outlasted subgrain formation and
439 fracturing. ~~Subgrains of less than 10 µm in size formed in the fracture plane (III in Fig. 5a).~~The
440 fractures described above are all crosscut by dilatant extensional fractures (set III in Fig. 5a),
441 oriented perpendicular to the stretching lineation and foliation, which do not show any
442 associated distortion of the crystal lattice.

443 The garnet porphyroclast of Figure 5c shows a central fracture as well as a set of two other
444 parallel fractures. The central fracture is the only one with significant offset and is filled with
445 kyanite and quartz. This fracture displays misorientations of more than 5° towards the right-
446 hand side of the scan, but none towards the left-hand side. In the lower left corner of the
447 fragment, subgrains are observed with misorientations, relative to the average orientation,
448 typically in the range of 10°. Misorientation axes are often parallel to (111) and (101). The
449 lowermost fragment shows a wide zone of progressive rotation. The chemical profile in Figure
450 5e shows the highest Ca counts towards the boundaries of the porphyroclasts and, internally,
451 towards two fractures. The larger fracture with apparent offset of the two garnet fragments
452 exhibits a less well-developed zone of calcium~~Ca enrichment~~efficient calcium diffusion when
453 compared to the tight fracture with introduced lattice distortion.



454

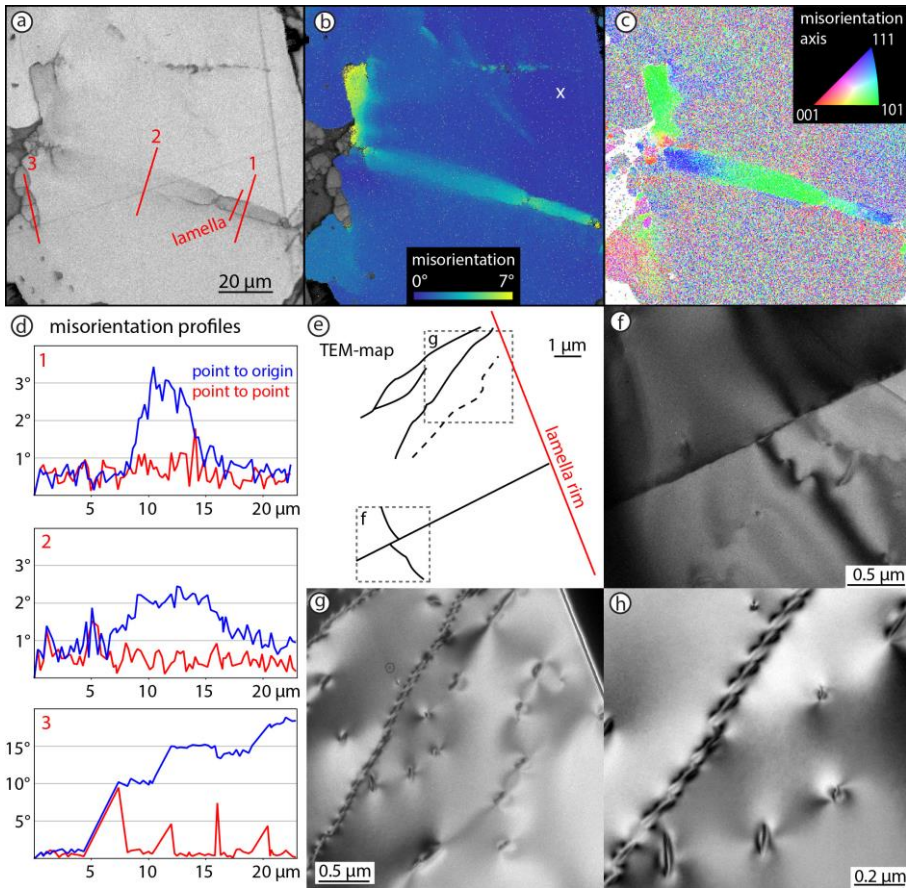
Figure 5: a) Inverse pole figure map of fractured garnet with three dominant orientations of fractures. b) Rose diagram correlating traced fracture orientations and (101)-planes for garnet in (a). c) Image quality map of a fragmented garnet with subgrains. d) Misorientation plot (with respect to the point marked with the white x) shows long wavelength bending in the lower fragment and distortion in the crystal lattice induced by a fracture in the upper fragment. e) EDS-calcium counts for the profile marked as a thin white line in (d).

455

456

457 3.5 TEM investigations

458 The garnet fragment of Figure 4g was further investigated using TEM, as it includes a narrow
459 zone of misorientation without fractures and is therefore suitable for preparation of FIB-
460 lamellae. As visible in Figure 6a (around profile 1), the image quality map shows a well-defined
461 narrow, darker [grey](#) band, possibly indicating high dislocation density. The zone is even
462 more evident in the misorientation plot (Fig. 6b) and changes from about 5 μm wide, with
463 discrete boundaries to the right, to a wider ($> 10 \mu\text{m}$) band towards the left of the image. In
464 the upper left part of the image, a subgrain boundary with $> 5^\circ$ misorientation transitions into
465 a zone of gradual misorientation. The misorientation axis is consistently parallel to (101) with
466 minor rotation around (111) (Fig. 6c, Fig. A2). Misorientation profiles reveal a slight
467 asymmetry within the narrow band, where the lower boundary appears to be sharper.
468 Misorientation changes more gradually within the wider portion of the misorientation band.
469 Locally, subgrains developed with discrete boundaries, documenting a misorientation of
470 usually around 5-10° (profile 3 in Fig. 6d). The FIB-lamella was cut across the narrow band of
471 misorientations (Fig. 6e). The lower boundary corresponds to a narrow discrete zone, without
472 visible dislocations (Fig. 6f). The upper boundary is marked by a series of dislocation walls and
473 only a few free dislocations are visible, which are often organized in arrays (Fig. 6g, h). The
474 existence of dislocation walls [and subgrain boundaries](#) indicates recovery by dislocation climb
475 [\(e.g., Hobbs, 1968; Passchier and Trouw, 2005\)](#).



476

Figure 6: a) Image quality map of the garnet fragment (compare Fig. 4f) with darker zones that can be interpreted as areas of high dislocation density and location of the FIB-lamella. b) Misorientation plot with respect to the reference point (marked with the white x) shows a discrete zone of misorientation, which has discrete boundaries in the right part of the image, but is more distributed towards the left. c) Misorientation axis plot with respect to the average orientation of the grain shows a consistent rotation around the (101) and (111) axes. For pole figure plots, see Fig. A2. d) Misorientation profiles indicated in a), for (1) the narrow zone, (2) the more distributed zone and (3) for subgrains. e) Overview sketch of the FIB-lamella used for TEM-analysis for correlation with the EBSD data. f) Sharp contrast boundary in the lower part of the lamella. g) Two dislocation walls with a few free dislocations, which are partly linking up parallel to the dislocation walls. h) Detail of the center-centre of (g)

477

478

479 **4 Discussion**

480 Garnets in this study show evidence for both brittle and ductile deformation under relatively
481 low temperatures of about 600 °C, as inferred from synchronous diffusion and ductile
482 shearing of pseudotachylyte (Hawemann et al, 2018). This is ~~well~~ below the experimentally
483 determined values for the onset of crystal-plastic deformation of garnet ([Wang and Ji, 1999](#))
484 ~~at the higher strain rates considered typical of mylonitic shear zones ($> 10^{-14} \text{ s}^{-1}$) ($> 850 \text{ °C}$;~~
485 ~~Wang and Ji, 1999)~~. In contrast to experiments, many natural examples (Vollbrecht et al.,
486 2006; Bestmann et al., 2008; Austrheim et al., 2017) indicate crystal plasticity of garnet at
487 lower temperatures between 650 °C and 700 °C, ~~challenging the reliability of extrapolation of~~
488 ~~experimental data to natural conditions.~~

489 The presence of microstructures and -textures consistent with dislocation climb and recovery,
490 as well as subgrain rotation, in garnet at around 600 °C is in agreement with previous studies
491 (Bestmann et al., 2008; Massey et al., 2011). No evidence for grain boundary sliding is
492 observed, since subgrains show rotation around a specific crystallographic axis. Rotation
493 around (111) and (101) is in accordance with the slip systems described by Voegelé et al.
494 (1998).

495 Multiple generations of overprinting fractures with different orientation demonstrate
496 repeated fracturing events. ~~Tensile-Extensional~~ fractures do not show any induced lattice
497 distortion or diffusion and therefore occurred after the temperature ~~was had decreased to~~
498 ~~values~~ too low for diffusion (Camacho et al., 2009), possibly during exhumation (compare
499 Prior, 1993 and Ji et al., 1997).

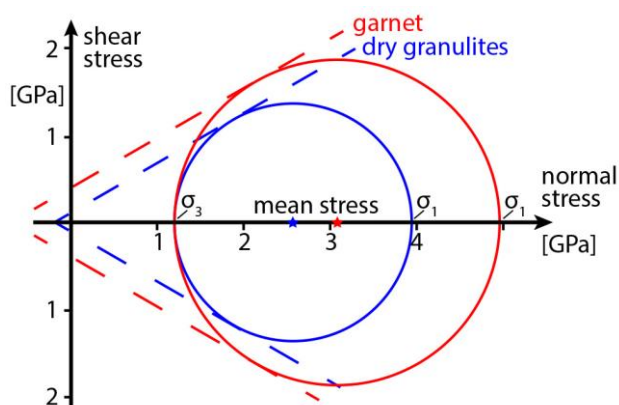
500 In contrast to the observations of Austrheim et al. (2017), ~~and~~ Papa et al. (2018) ~~and Petley-~~
501 ~~Ragan et al. (2019)~~ from other examples in the deep continental crust, no “explosive

502 fracturing” ~~of~~ “shattering” or “fragmentation” of garnet is observed in relict porphyroclasts
503 immediately adjacent to pseudotachylyte. The fractures described here are generally planar
504 and often consistently oriented, in some cases showing single and conjugate shear offsets.
505 Fractured garnet is not restricted to the boundary with pseudotachylyte and is still present
506 even in samples without pseudotachylyte, where the nearest pseudotachylyte is possibly
507 many ~~meters~~ metres or more away. Fracturing in this case cannot be related to thermal shock
508 (Papa et al., 2018) or localized high stress due to (seismic) fracture propagation (Austrheim et
509 al., 2017; Petley-Ragan et al., 2019), but must reflect a larger scale distribution of differential
510 stresses in the lower crust that were, at least transiently, high enough to cause brittle garnet
511 failure (Hawemann et al., 2019). This could be due to stress pulses from earthquakes in the
512 shallower brittle regime (Trepmann and Stöckhert, 2002; Ellis and Stöckhert, 2004; Jamtveit
513 et al., 2018a, b; Jamtveit et al., in press) or a more local, lower crustal source due to jostling
514 of less-deformed strong blocks within an irregular shear zone network (Hawemann et al.,
515 2019).
516 The narrower Ca diffusion profiles on some fractures relative to garnet rims and crosscutting
517 relationships suggest that fracturing was recurrent under sub-eclogite facies metamorphic
518 conditions, as also indicated by the occasional presence of kyanite in ~~some of~~ some fractures.
519 The presence of kyanite needles and the absence of zoisite/clinozoisite or epidote, as a
520 breakdown product of plagioclase during sub-eclogitic metamorphism (Fig. 3b), indicate
521 relatively dry lower crustal conditions (Hawemann et al., 2018). According to Wayte et al.
522 (1989), this indicates a water activity of < 0.004, calculated for rocks of comparable
523 composition and P-T conditions. However, new biotite did form in ~~dilatant~~ fractures across
524 relict garnet, so conditions were probably not strictly anhydrous. The sheared and
525 recrystallized pseudotachylyte developed a similar synkinematic assemblage as the host

526 mylonite, demonstrating that there is also no marked partitioning of water into the frictional
527 melt, which implies little free or bound water available in the original source rock (e.g. Wex
528 et al., 2018). The effect of pore-fluid pressure on the effective confining pressure must
529 therefore have been negligible.

530 As reported in Hawemann et al. (2019), the dynamically recrystallized quartz grain size and
531 microstructure in the host rock mylonites indicates that long-term flow stresses were not
532 particularly high, on the order of less than 10 MPa. The ambient pressure of ca. 1.1-1.2 GPa
533 determined for the host rocks should therefore be close to the lithostatic value (Mancktelow,
534 2008). Figure 7 shows a simple linear plot of the Mohr-Coulomb failure criterion for an angle
535 of internal friction of 30° (coefficient $\mu = 0.6$), a lithostatic load of 1.2 GPa, and no pore fluid
536 pressure. This plot is only qualitative, since the angle of internal friction could decrease
537 towards higher pressure ([Shimada et al., 1983](#)). However, the summary of experimental
538 results in Byerlee (1978) indicates that there may be little change at least up to pressures
539 similar to those considered here. It follows that the differential stress for fracture initiation
540 must have been of the same order as the confining pressure (Fig. 7). As discussed in detail in
541 Hawemann et al. (2019), such high differential stresses, leading to garnet fracture and the
542 development of abundant pseudotachylyte, can only have been transient and presumably
543 related to repeated short-term seismic events in the lower continental crust ([Hawemann et](#)
544 [al., 2018](#); [Jamtveit et al, 2018a, b](#); [Menegon et al., 2017](#)). The lack of shattered garnet adjacent
545 to pseudotachylyte in these samples may reflect drier conditions relative to those in the
546 Bergen Arc (Austrheim et al., 2017) and Mont Mary (Papa et al., 2018). The samples studied
547 could therefore represent one end-member of the lower continental crust, where
548 deformation occurs without the initial presence or influx of free water during fracturing and
549 subsequent crystal-plastic deformation.

550



551

Figure 7: Mohr circles for fracturing of dry granulites and garnet at 1.2 GPa lithostatic load

552

553 5 Conclusions

554 In dry lower continental crust deformed under conditions of ca. 600 °C and 1.1 GPa, garnet
555 shows both single and conjugate sets of shear fractures, fractures with associated subgrains
556 and induced lattice damage around fractures, subgrain formation without fracturing, and
557 late-stage ~~dilatant~~-extensional fractures. Most of these fractures show a strong
558 crystallographic control, with fracturing preferentially occurring along the (101) planes of
559 garnet. Dynamic recrystallization is evident from inferred subgrain rotation recrystallization
560 and recovery is manifested by the presence of dislocation walls. The observed
561 microstructures of garnets are interpreted to record transient high stresses during deep
562 seismic events in the lower crustal Fregon Subdomain. ~~This~~ which is also indicated by the
563 abundant occurrence of pseudotachylyte developed under similar lower crustal conditions
564 and, possibly, by the variability of recrystallized quartz grain sizes including values down to a
565 few ~~micrometers~~micrometres (Hawemann et al. 2009b). The studied example represents one

566 end-member of lower continental crustal ~~behavior~~behaviour where, because of earlier
567 metamorphic dehydration and the intracratonic position well removed from the plate margin,
568 rocks were initially dry and water was not introduced during fracturing and crystal-plastic
569 deformation.

570 Author contributions

571 All authors listed took part in at least two of the three field seasons. NM assisted FH in the data
572 collection and interpretation. AC's and GP's knowledge in the field of garnet deformation and diffusion
573 processes were crucial in preparing the manuscript. SW contributed to the microprobe and SEM work.
574 FH prepared the manuscript with contributions from all co-authors.

575 Competing interests

576 The authors declare that they have no conflict of interest.

577

578 **Acknowledgements**

579 We want to thank Matthias Konrad-Schmolke and an anonymous reviewer for their critical
580 comments which improved the manuscript. We gratefully acknowledge permission granted to
581 work on the Anangu Pitjantjatjara Yankunytjatjara Lands (APY) to carry out our field work in
582 the area. The Northern Territory Geological Survey (NTGS) and Basil Tikoff (Department of
583 Geoscience, University of Wisconsin) are thanked for their logistical support and the Nicolle
584 family of Mulga Park station for their hospitality. The Scientific Center for Optical and Electron
585 Microscopy (ScopeM) provided the facilities for the scanning electron microscopy work, and
586 help by Karsten Kunze, Luiz Morales and Fabian Gramm is especially acknowledged. Luca
587 Menegon is thanked for his review of the first author's doctoral thesis. This project was
588 financed by the Swiss National Science Foundation (SNF) grant 200021_146745 and by the

589 University of Padova (BIRD175145/17: The geological record of deep earthquakes: the
590 association pseudotachylyte-mylonite).

591

592 **Data ~~Availability~~Availability**

593 All data used in this paper can be accessed through the depository of the Open Science

594 Framework here: <https://osf.io/yrzgh/>

595

596 **References**

597 Austrheim, H., Erambert, M. and Boundy, T. M.: Garnets recording deep crustal earthquakes, *Earth
598 and Planetary Science Letters*, 139(1–2), 223–238, doi:10.1016/0012-821X(95)00232-2, 1996.

599 Austrheim, H., Dunkel, K. G., Plümper, O., Ildefonse, B., Liu, Y. and Jamtveit, B.: Fragmentation of
600 wall rock garnets during deep crustal earthquakes, *Science Advances*, 3(2), e1602067,
601 doi:10.1126/sciadv.1602067, 2017.

602 [Angiboust, S., Yamato, P., Hertgen, S., Hyppolito, T., Bebout, G.E., Morales, L.: Fluid pathways and
603 high-P metasomatism in a subducted continental slice \(Mt. Emilius klippe, W. Alps\), *Journal of
604 Metamorphic Geology*, 35, 471–492, 2017.](#)

605 Baxter, E. F. and Scherer, E. E.: Garnet Geochronology: Timekeeper of Tectonometamorphic
606 Processes, *Elements*, 9(6), 433–438, doi:10.2113/gselements.9.6.433, 2013.

607 [Behr, W.M., Platt, J.P., 2011: A naturally constrained stress profile through the middle crust in an
608 extensional terrane. *Earth and Planetary Science Letters* 303, 181-192, 2011.](#)

609 Bell, T. H.: Progressive deformation and reorientation of fold axes in a ductile mylonite zone: the
610 Woodroffe thrust, *Tectonophysics*, 44(1), 285–320, 1978.

611 Bestmann, M., Habler, G., Heidelbach, F. and Thöni, M.: Dynamic recrystallization of garnet and
612 related diffusion processes, *Journal of Structural Geology*, 30(6), 777–790,
613 doi:10.1016/j.jsg.2008.02.007, 2008.

614 Caddick, M. J., Konopasek, J. and Thompson, A. B.: Preservation of Garnet Growth Zoning and the
615 Duration of Prograde Metamorphism, *Journal of Petrology*, 51(11), 2327–2347,
616 doi:10.1093/petrology/egq059, 2010.

617 Camacho, A. and Fanning, C. M.: Some isotopic constraints on the evolution of the granulite and
618 upper amphibolite facies terranes in the eastern Musgrave Block, central Australia, *Precambrian
619 Research*, 71(1), 155–181, 1995.

620 Camacho, A. and Fitz Gerald, J. D.: Misidentification of oxide phases and of twinned kyanite:
621 implications for inferred P-T histories of the Musgrave Block, central Australia, *Journal of the Virtual*
622 *Explorer*, 35, doi:10.3809/jvirtex.2011.00275, 2010.

623 Camacho, A., Vernon, R. H. and Fitz Gerald, J. D.: Large volumes of anhydrous pseudotachylyte in the
624 Woodroffe Thrust, eastern Musgrave Ranges, Australia, *Journal of Structural Geology*, 17(3), 371–
625 383, 1995.

626 Camacho, A., Compston, W., McCulloch, M. and McDougall, I.: Timing and exhumation of eclogite
627 facies shear zones, Musgrave Block, central Australia, *J. metamorphic Geol.*, 15, 735–751, 1997.

628 Camacho, A., Yang, P. and Frederiksen, A.: Constraints from diffusion profiles on the duration of
629 high-strain deformation in thickened crust, *Geology*, 37(8), 755–758, 2009.

630 Collerson, K. D., Oliver, R. L. and Rutland, R. W. R.: An example of structural and metamorphic
631 relationships in the Musgrave orogenic belt, central Australia, *Journal of the Geological Society of*
632 *Australia*, 18(4), 379–393, doi:10.1080/00167617208728776, 1972.

633 Dalziel, I. W. D. and Bailey, S. W.: Deformed garnets in a mylonitic rock from the Grenville Front and
634 their tectonic significance, *American Journal of Science*, 266(7), 542–562, doi:10.2475/ajs.266.7.542,
635 1968.

636 [Ellis, S., Stöckhert, B.: Elevated stresses and creep rates beneath the brittle-ductile transition caused](#)
637 [by seismic faulting in the upper crust. *Journal of Geophysical Research*, 109, B05407, 2017.](#)

638 [Engi, M., Giuntoli, F., Lanari, P., Burn, M., Kunz, B. E., and Bouvier, A.-S.: Pervasive eclogitization due](#)
639 [to brittle deformation and rehydration of subducted basement: Effects on continental recycling?,](#)
640 [Geochemistry Geophysics Geosystems, 19, <https://doi.org/10.1002/2017GC007215>, 2018.](#)

641 Evins, P. M., Smithies, R. H., Howard, H. M., Kirkland, C. L., Wingate, M. T. D. and Bodorkos, S.:
642 Redefining the Giles Event within the setting of the 1120-1020 Ma Ngaanyatjarra Rift, West
643 Musgrave Province, Central Australia, *Geological Society of Western Australia*, East Perth, W.A.,
644 2010.

645 Gray, C. M.: Geochronology of granulite - facies gneisses in the western Musgrave Block, Central
646 Australia, *Journal of the Geological Society of Australia*, 25(7–8), 403–414,
647 doi:10.1080/00167617808729050, 1978.

648 [Giuntoli, F., Lanari, P., and Engi, M.: Deeply subducted continental fragments – Part 1: Fracturing,](#)
649 [dissolution–precipitation, and diffusion processes recorded by garnet textures of the central Sesia](#)
650 [Zone \(western Italian Alps\), *Solid Earth*, 9, 167–189, <https://doi.org/10.5194/se-9-167-2018>, 2018.](#)

651 Hawemann, F., Mancktelow, N. S., Wex, S., Camacho, A. and Pennacchioni, G.: Pseudotachylyte as
652 field evidence for lower-crustal earthquakes during the intracontinental Petermann Orogeny
653 (Musgrave Block, Central Australia), *Solid Earth*, 9(3), 629–648, doi:10.5194/se-9-629-2018, 2018.

654 Hawemann, F., Mancktelow, N. S., Pennacchioni, G., Wex, S. and Camacho, A.: Weak and slow,
655 strong and fast: How shear zones evolve in a dry continental crust (Musgrave Ranges, Central
656 Australia), *Journal of Geophysical Research: Solid Earth*, doi:10.1029/2018JB016559, 2019.

657 [Hobbs, B.E.: Recrystallisation of single crystals of quartz. *Tectonophysics*, 6, 353-401, 1968.](#)

658 Hofer, H. E. and Brey, G. P.: The iron oxidation state of garnet by electron microprobe: Its
659 determination with the flank method combined with major-element analysis, *American*
660 *Mineralogist*, 92(5–6), 873–885, doi:10.2138/am.2007.2390, 2007.

661 [Jamtveit, B., Ben-Zion, Y., Renard, F., Austrheim, H., 2018: Earthquake-induced transformation of](#)
662 [the lower crust. *Nature* 556, 487-491, 2018a.](#)

663 [Jamtveit, B., Moulas, E., Andersen, T.B., Austrheim, H., Corfu, F., Petley-Ragan, A., Schmalholz, S.M.:](#)
664 [High pressure metamorphism caused by fluid induced weakening of deep continental crust.](#)
665 [*Scientific Reports*, 8, 17011, 2018b.](#)

666 [Jamtveit, B., Petley-Ragan, A., Incel, S., Dunkel, K.G., Aupart, C., Austrheim, H., Corfu, F., Menegon, L.,](#)
667 [Renard, F.: The effects of earthquakes and fluids on the metamorphism of the lower continental](#)
668 [crust, *Journal of Geophysical Research: Solid Earth*, doi:10.1029/2018jb016461, in press.](#)

669

670 Ji, S., Zhao, P. and Saruwatari, K.: Fracturing of garnet crystals in anisotropic metamorphic rocks
671 during uplift, *Journal of Structural Geology*, 19(5), 603–620, 1997.

672 Karato, S., Wang, Z., Liu, B. and Fujino, K.: Plastic deformation of garnets: systematics and
673 implications for the rheology of the mantle transition zone, *Earth and Planetary Science Letters*,
674 130(1–4), 13–30, 1995.

675 Kirkpatrick, J. D. and Rowe, C. D.: Disappearing ink: How pseudotachylytes are lost from the rock
676 record, *Journal of Structural Geology*, 52, 183–198, doi:10.1016/j.jsg.2013.03.003, 2013.

677 [Konrad-Schmolke, M., O'Brien, P. J., Heidelberg, F.: Compositional reequilibration of garnet: the](#)
678 [importance of sub-grain boundaries. *European Journal of Mineralogy* 19, 431–438, 2007.](#)

679 Kunze, K., Wright, S. I., Adams, B. L. and Dingley, D. J.: Advances in automatic EBSD single orientation
680 measurements, *Texture, Stress, and Microstructure*, 20(1–4), 41–54, 1993.

681 Lasaga, A. C.: Geospeedometry: an extension of geothermometry, in *Kinetics and equilibrium in*
682 *mineral reactions*, pp. 81–114, Springer. [online] Available from:
683 http://link.springer.com/chapter/10.1007/978-1-4612-5587-1_3 (Accessed 28 May 2017), 1983.

684 Major, R. B.: Explanatory Notes for the Woodroffe 1: 250 000 Geological Map SG/52-12 (1st
685 ed.). Adelaide, Australia: Geological Survey of South Australia, 1973.

686 Massey, M. A., Prior, D. J. and Moecher, D. P.: Microstructure and crystallographic preferred
687 orientation of polycrystalline microgarnet aggregates developed during progressive creep, recovery,
688 and grain boundary sliding, *Journal of Structural Geology*, 33(4), 713–730,
689 doi:10.1016/j.jsg.2010.12.009, 2011.

690 [Menegon, L., Pennacchioni, G., Malaspina, N., Harris, K., & Wood, E., 2017: Earthquakes as](#)
691 [precursors of ductile shear zones in the dry and strong lower crust. *Geochemistry, Geophysics,*](#)
692 [*Geosystems*, 18. <https://doi.org/10.1002/2017GC007189>, 2017.](#)

693 Papa, S., Pennacchioni, G., Angel, R. J. and Faccenda, M.: The fate of garnet during (deep-seated)
694 coseismic frictional heating: The role of thermal shock, *Geology*, 46(5), 471–474,
695 doi:10.1130/G40077.1, 2018.

696 [Passchier, C.W., Trouw, R.A.J.: *Microtectonics \(2nd Edition\)*, Springer, Heidelberg, 366 pp., 2005.](#)

697 [Petley-Ragan, A., Dunkel, K. G., Austrheim, H., Ildefonse, B., Jamtveit, B.: Microstructural records of](#)
698 [earthquakes in the lower crust and associated fluid-driven metamorphism in plagioclase-rich](#)
699 [granulites. *Journal of Geophysical Research: Solid Earth*, 123, 3729–3746.](#)
700 <https://doi.org/10.1029/2017JB015348>, 2018

701 [Petley-Ragan, A., Ben-Zion, Y., Austrheim, H., Ildefonse, B., Renard, F., Jamtveit, B.: Dynamic](#)
702 [earthquake rupture in the lower crust. *Science Advances*, 5, doi: 10.1126/sciadv.aaw0913, 2019.](#)

703 Prior, D. J.: Sub-critical fracture and associated retrogression of garnet during mylonitic deformation,
704 *Contributions to Mineralogy and Petrology*, 113(4), 545–556, doi:10.1007/BF00698322, 1993.

705 Prior, D. J., Wheeler, J., Brenker, F. E., Harte, B. and Matthews, M.: Crystal plasticity of natural
706 garnet: New microstructural evidence, *Geology*, 28(11), 1003, doi:10.1130/0091-
707 7613(2000)28<1003:CPONGN>2.0.CO;2, 2000.

708 Prior, D. J., Wheeler, J., Peruzzo, L., Spiess, R. and Storey, C.: Some garnet microstructures: an
709 illustration of the potential of orientation maps and misorientation analysis in microstructural
710 studies, *Journal of Structural Geology*, 24(6–7), 999–1011, doi:10.1016/S0191-8141(01)00087-6,
711 2002.

712 Raimondo, T., Collins, A. S., Hand, M., Walker-Hallam, A., Smithies, R. H., Evins, P. M. and Howard, H.
713 M.: The anatomy of a deep intracontinental orogen, *Tectonics*, 29(4), n/a-n/a,
714 doi:10.1029/2009TC002504, 2010.

715 [Shimada, M., Cho, A., Yukutake, H., 1983: Fracture strength of dry silicate rocks at](#)
716 [high confining pressures and activity of acoustic emission. *Tectonophysics* 96, 159–](#)
717 [172. doi:10.1016/0040-1951\(83\)90248-2, 1983.](#)

718

719 Sibson, R. H.: Generation of pseudotachylite by ancient seismic faulting, *Geophysical Journal*
720 *International*, 43(3), 775–794, 1975.

721 Sibson, R. H. and Toy, V. G.: The habitat of fault-generated pseudotachylite: Presence vs. absence of
722 friction-melt, in *Geophysical Monograph Series*, vol. 170, edited by R. Abercrombie, A. McGarr, H.
723 Kanamori, and G. Di Toro, pp. 153–166, American Geophysical Union, Washington, D. C. [online]
724 Available from: <http://www.agu.org/books/gm/v170/170GM16/170GM16.shtml> (Accessed 21
725 January 2014), 2006.

726 Toy, V. G., Ritchie, S. and Sibson, R. H.: Diverse habitats of pseudotachylites in the Alpine Fault Zone
727 and relationships to current seismicity, *Geological Society, London, Special Publications*, 359(1), 115–
728 133, doi:10.1144/SP359.7, 2011.

729 Trepmann, C. A. and Stöckhert, B.: Cataclastic deformation of garnet: a record of synseismic loading
730 and postseismic creep, *Journal of Structural Geology*, 24(11), 1845–1856, doi:10.1016/S0191-
731 8141(02)00004-4, 2002.

732 Voegelé, V., Cordier, P., Sautter, V., Sharp, T. G., Lardeaux, J. M. and Marques, F. O.: Plastic
733 deformation of silicate garnets, *Physics of the Earth and Planetary Interiors*, 108(4), 319–338,
734 doi:10.1016/S0031-9201(98)00111-3, 1998.

735 Vollbrecht, A., Pawlowski, J., Leiss, B., Heinrichs, T., Seidel, M. and Kronz, A.: Ductile deformation of
736 garnet in mylonitic gneisses from the Münchberg Massif (Germany), *Tectonophysics*, 427(1–4), 153–
737 170, doi:10.1016/j.tecto.2006.05.024, 2006.

- 738 Wang, Z. and Ji, S.: Deformation of silicate garnets; brittle-ductile transition and its geological
739 implications, *The Canadian Mineralogist*, 37(2), 525, 1999.
- 740 Wayte, G. J., Worden, R. H., Rubie, D. C. and Droop, G. T. R.: A TEM study of disequilibrium
741 plagioclase breakdown at high pressure: the role of infiltrating fluid, *Contributions to Mineralogy
742 and Petrology*, 101(4), 426–437, doi:10.1007/BF00372216, 1989.
- 743 Wex, S., Mancktelow, N. S., Hawemann, F., Camacho, A. and Pennacchioni, G.: Geometry of a large-
744 scale, low-angle, mid-crustal thrust (Woodroffe Thrust, central Australia): Geometry of a mid-crustal
745 thrust, *Tectonics*, doi:10.1002/2017TC004681, 2017.
- 746 Wex, S., Mancktelow, N. S., Hawemann, F., Camacho, A. and Pennacchioni, G.: Inverted distribution
747 of ductile deformation in the relatively “dry” middle crust across the Woodroffe Thrust, central
748 Australia, *Solid Earth*, 9(4), 859–878, doi:10.5194/se-9-859-2018, 2018.
- 749 Wex, S., Mancktelow, N. S., Camacho, A. and Pennacchioni, G.: Interplay between seismic fracture
750 and aseismic creep in the Woodroffe Thrust, central Australia – Inferences for the rheology of
751 relatively dry continental mid-crustal levels, *Tectonophysics*, 758, 55–72,
752 doi:10.1016/j.tecto.2018.10.024, 2019.

753

754

755

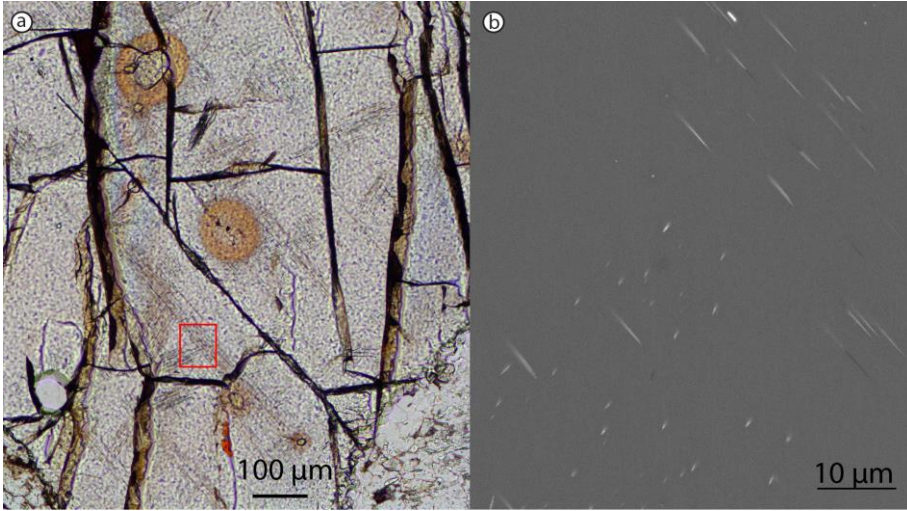
756

757

758

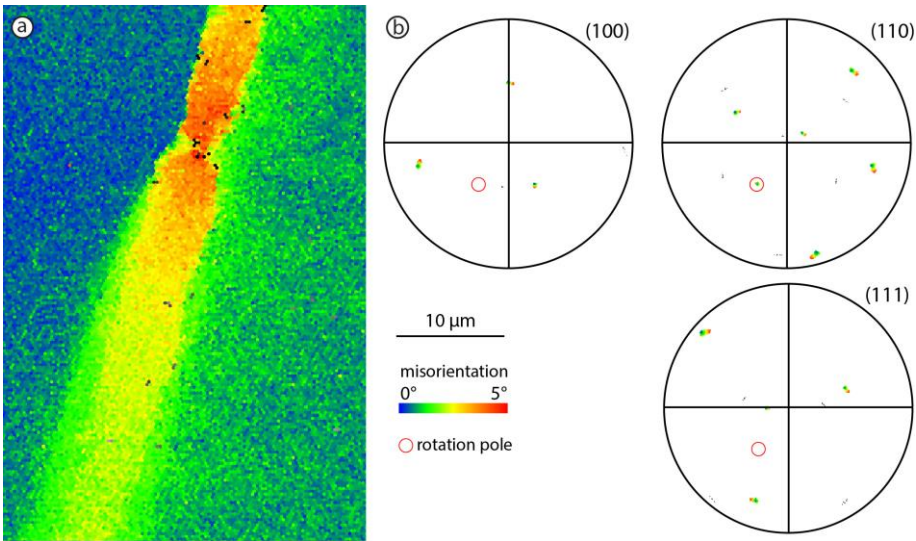
759

760 **Appendix**



761

762 *Figure A1: Thin section image in plane polarized light of a garnet crystal with monazite*
 763 *inclusions (with halos) and rutile-exsolution needles. b) BSE-image of the area indicated with*
 764 *the red box.*



765

766 Figure A2: a) Misorientation map-detail for Fig. 6b), with b) pole figure plots for garnet axis
767 with the same ~~color~~colour scheme. The plots reveal a rotation around a (101)-axis, as indicated
768 by the red circle.